remote sensing

MDPI

Article

Analysis of BDS/GPS Signals' Characteristics and Navigation Accuracy for a Geostationary Satellite

Meng Wang [1,2,*], Tao Shan [1], Wanwei Zhang [3] and Hao Huan [1]

[1] School of Information and Electronics, Beijing Institute of Technology, No. 5 South Street, Zhongguancun, Haidian District, Beijing 100081, China; shantao@bit.edu.cn (T.S.); huanhao@bit.edu.cn (H.H.)
[2] Department of Navigation, Beijing Institute of Satellite Information Engineering (Aerospace Star Technology Co., Ltd), 77 Jindai Road, Zhongguancun, Haidian District, Beijing 100095, China
[3] School of Geodesy and Geomatics, Wuhan University, Wuhan 430079, China; wwzhang@sgg.whu.edu.cn
* Correspondence: 3120170387@bit.edu.cn

Abstract: The utilization of Global Navigation Satellite System (GNSS) is becoming an attractive navigation approach for geostationary orbit (GEO) satellites. A high-sensitivity receiver compatible with Global Position System (GPS) developed by the United States and BeiDou Navigation Satellite System (BDS) developed by China has been used in a GEO satellite named TJS-5 to demonstrate feasibility of real-time navigation. According to inflight data, the GNSS signal characteristics including availability, position dilution of precision (PDOP), carrier-to-noise ratio (C/N_0), observations quantity and accuracy are analyzed. The mean number of GPS and GPS + BDS satellites tracked are 7.4 and 11.7 and the mean PDOP of GPS and GPS + BDS are 10.24 and 3.91, respectively. The use of BDS significantly increases the number of available navigation satellites and improves the PDOP. The number of observations with respect to C/N_0 is illustrated in detail. The standard deviation of the pseudorange noises are less than 4 m, and the corresponding carrier phase noises are mostly less than 8 mm. We present the navigation performance using only GPS observations and GPS + BDS observations combination at different weights through comparisons with the precision reference orbits. When GPS combined with BDS observations, the root mean square (RMS) of the single-epoch least square position accuracy can improve from 32.1 m to 16.5 m and the corresponding velocity accuracy can improve from 0.238 m/s to 0.165 m/s. The RMS of real-time orbit determination position accuracy is 5.55 m and the corresponding velocity accuracy is 0.697 mm/s when using GPS and BDS combinations. Especially, the position accuracy in x-axis direction reduced from 7.24 m to 4.09 m when combined GPS with BDS observations.

Keywords: GEO; GPS; BDS; orbit determination; navigation

Citation: Wang, M.; Shan, T.; Zhang, W.; Huan, H. Analysis of BDS/GPS Signals' Characteristics and Navigation Accuracy for a Geostationary Satellite. *Remote Sens.* **2021**, *13*, 1967. https://doi.org/10.3390/rs13101967

Academic Editors: Jay Hyoun Kwon, Chang-Ki Hong and Tae-Suk Bae

Received: 11 April 2021
Accepted: 14 May 2021
Published: 18 May 2021

1. Introduction

Nowadays, real-time orbit determination based on GNSS is successfully used for GEO satellites which traditionally depended on ground-based ranging systems. Because of the advantages of cost-effectiveness and autonomy, the utilization of GNSS receivers in GEO missions has become an attractive alternative for orbit determination and timing. In the 1980s, the concept of using GPS on GEO satellite has been introduced. In 2000, the United States released the operational requirements document (ORD) and presented the first description of space service volume (SSV), which was a shell extending from 3000 km altitude to approximately the GEO altitude, or 36,000 km [1,2]. In 2006, Bauer formally described the concept of SSV, and made it clear that SSV coverage characteristic with the GPS constellation [2]. Recently, considerable effort has been exerted by the United Nations-sponsored International Committee on GNSS (ICG) to expand the GNSS use into the SSV, by conducting initiatives to ensure GNSS signals available in the SSV. ICG is leading to coordinate the development of an interoperable SSV across the navigation service provider, including GPS, BDS, Galileo, GLONASS, etc. [3,4]. An analysis of the BDS-3 performance

of the main-lobe and the side-lobe signals for three typical SSV missions is conducted based on antenna patterns from the actual mission design data [5,6].

However, the use of GNSS signals for SSV users has special challenges. Several researches have carried out studies in signal link budgets and performance for SSV applications. In GEO missions, the altitude of GNSS receiver is higher than that of the navigation satellite constellation and the geometric distribution of the navigation satellite is poor. Most of the signals from the main lobe of the GNSS transmitting antenna are blocked by the earth [7–9]. It is necessary to receive the side lobe signals to increase the number of available navigation satellites and improve the geometric distribution [9]. Because the power of side-lobe signals are generally about 20 dB lower than that of the main-lobe ones, we need to improve sensitivity of the receiver to process these signals [10–12]. In spite of these difficulties, several feasibility studies for orbit determination with GNSS in GEO missions have been presented. A software simulation was made to assess the performance of autonomous orbit determination using GPS and Galileo signals. The accuracy of GEO orbit determination in this simulation was less than 100 m [13]. An iterative Kalman filter based on nonlinear dynamic model was used with GPS measurements for GEO spacecraft navigation. The tests of this filter were conducted with a GPS signal simulator and a dual-star single-frequency receiver [14]. Comprehensive simulation results and analysis show that using GPS and Galileo navigation for GEO orbits has operational benefits, even current space borne state-of-the-art receivers are considered [15]. A system-level performance and qualification test for GEO missions has been conducted using a space borne GPS receiver, named General Dynamics' Viceroy-4. It has demonstrated the ability to provide 100% position, velocity, and time data by acquiring and tracking a significant number of side lobe signals [11]. GNSS signal characteristics in GEO, taking into consideration the L1 and L5 frequency bands and the GPS and Galileo constellations, are specifically investigated. Simulation tests and experiments using a high sensitivity commercial off-the-shelf (COTS) receiver were presented to validate the navigation performance [16].

Moreover, several missions have demonstrated the flight performance of GNSS signal processing and onboard orbit determination in GEO orbit. In Europe, Galileo navigation satellite GIOVE-A with a SGR-GEO receiver and an experimental results show that weak side lobe signals have been acquired and tracked by this receiver to increase the number of available satellites in medium-earth-orbit (MEO) and GEO. The position accuracy in this experiment was less than 100 m [17,18]. The Geostationary Operational Environmental Satellite-R (GOES-R) adopts Viceroy-4 as an onboard GPS receiver to provide orbit determination data for guidance, navigation, and control systems [19]. According to on-orbit performance, the position accuracy is less than 15.2 m and the velocity accuracy is less than 0.52 cm/s [20]. In Europe, a receiver Mosaic GNSS has been adopted in SmallGEO platform used in the Hispasat 36W-1 mission. The flight results show that signals with C/N_0 at 27dB-Hz–28 dB-Hz are received and the RMS of position error is around 120 m [21]. In a GEO mission of TJS-2, the onboard receiver can track 6–8 GPS satellites and the minimum C/N_0 of signals tracked was 24 dB-Hz. The RMS of position error between 30 h orbit determination arcs is 2.14 m using the overlap comparisons assessment [22]. Furthermore, several publications have addressed the feasibility of GNSS-based navigation for lunar missions. Navigation results obtained with a realistic simulator were presented by the past studies to demonstrate the feasibility of lunar orbit spacecraft applications that rely on GNSS receivers [23,24].

The GEO satellite of No.5 Telecommunication Technology Test Satellite (TJS-5) was launched on 7 January 2020, and a high sensitivity GNSS receiver has been installed to realize tracking GPS and BDS signals and to perform orbit determination autonomously. In this study, we investigate the flight signal characteristics in this GEO missions, considering GPS and BDS in terms of availability, PDOP, C/N_0, the observation quantity and accuracy. Then, we give the performance evaluation of single-epoch least square solutions and real–time orbit determination solutions and discuss the contribution of BDS signals to GEO applications.

2. System and Methods Description

In the GEO satellite of TJS-5 experiment, the altitude of the receiver is higher than that of the MEO navigation satellite, as shown in Figure 1. Therefore the GNSS receiver receives the signals from the other side of the earth and the elevation of this receiver is negative. A high-gain antenna in form of bifilar helix mounted in a deployable structure is oriented toward the center of the earth. The gain of this antenna is more than 7 dB within an angle of −30°–+30° according to the measured data. It should be noted that the BDS GEO/IGSO satellites and receiver are on the same orbital plane over the Asia Pacific. The elevation of these BDS GEO/IGSO satellites is beyond the beam range of the receiving antenna (−30°–+30°). In this situation, whether BDS GEO/IGSO satellites signal can be received or not depends on the signal transmission distance, the side-lobe gain of the navigation satellite antenna and the receiving antenna gain.

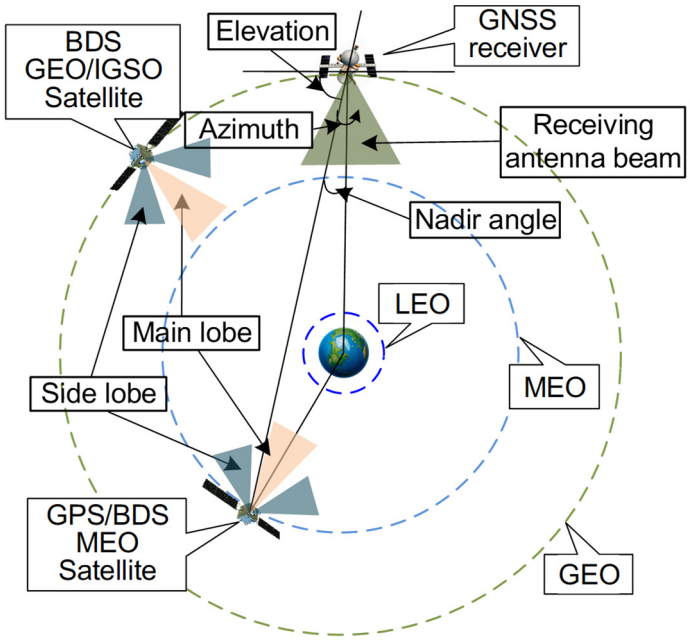

Figure 1. Reception geometry for MEO, IGSO and GEO navigation satellites and receiver in GEO mission.

A high-sensitivity receiver are used for acquisition and tracking the weak navigation signals in this experiment. Table 1 provides some information about this GNSS receiver. The architecture of this high-sensitivity spaceborne receiver is shown in Figure 2. The filter, low noise amplifier (LNA), and the RF-front ends downconvert the navigation signals to intermediate frequency (IF) signals which are sampled at 56.8 MHz. The RF-front is driven by a stable, low-phase noise, 10MHz oven-controlled crystal oscillator (OXCO). The high sensitivity fast acquisition and tracking are performed in the digital application specific integrated circuit (ASIC), which is embedded in a rad-hard system on chip (SOC). Raw measurements (pseudorange, carrier phase, ephemeris, time, etc.) are generated and used for the single point position and real-time orbit determination by the CPU in this SOC. The receiver can track up to eight GPS satellites and eight BDS satellites with 16-channel hardware correlators simultaneously. A real-time orbit determination filter based on an extended Kalman filter (EKF) in this receiver works with pseudorange observations and dynamic models.

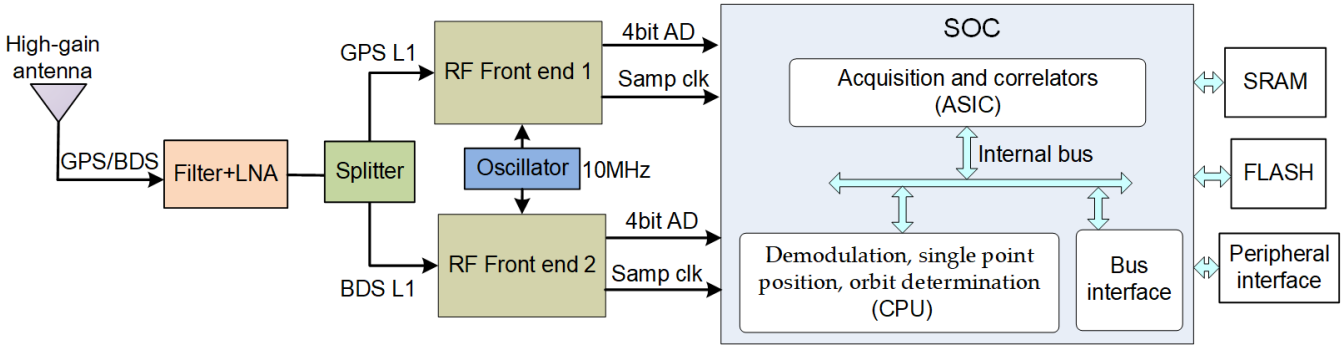

Figure 2. Block diagram of the BDS and GPS receiver architecture.

Table 1. Primary parameters of the TJS-5 spaceborne receiver.

Parameters	Value
Compatible frequency	BDS B1I, GPS L1 C/A
Number of channels	8 for BDS, 8 for GPS
Original observation types	Carrier phase, pseudorange and C/N_0
Acquisition sensitivity	28 dB-Hz
Tracking sensitivity	24 dB-Hz
OXCO accuracy	0.5 ppm
OXCO Allan variance	$\leq 1 \cdot 10^{-11}$ s^{-1}

This receiver can process L1 C/A signals of 32 GPS satellites of the PRN G01–G32. Moreover, this receiver can be compatible with the BeiDou regional system (BDS-2) and the BeiDou global system (BDS-3), which have three orbit types: medium earth orbit (MEO), inclined geostationary orbit (IGSO), and GEO [25,26]. The receiver can process the B1I signals of 37 BDS satellites of the PRN C01–C37. Because C15, C17, C18 and C31 satellites are out of service, there are 33 BDS satellites which can be tracked by the receiver, including 5 BDS-2 GEO, 7 BDS-2 IGSO, 3 BDS-2 MEO, and 18 BDS-3 MEO satellites, as listed in Table 2.

Table 2. Status of healthy BDS satellites can be used by the receiver.

BDS-3			BDS-2		
PRN	**Common**	**Date**	**PRN**	**Common**	**Date**
C19	MEO-1	5 November 2017	C1	GEO-1	16 January 2010
C20	MEO-2	5 November 2017	C2	GEO-6	25 October 2012
C21	MEO-3	12 February 2018	C3	GEO-7	12 June 2016
C22	MEO-4	12 February 2018	C4	GEO-4	1 November 2010
C23	MEO-5	29 July 2018	C5	GEO-5	25 February 2012
C24	MEO-6	29 July 2018	C6	IGSO-1	1 August 2010
C25	MEO-11	25 August 2018	C7	IGSO-2	18 December 2010
C26	MEO-12	25 August 2018	C8	IGSO-3	10 April 2011
C27	MEO-7	12 January 2018	C9	IGSO-4	27 July 2011
C28	MEO-8	12 January 2018	C10	IGSO-5	2 December 2011
C29	MEO-9	30 March 2018	C11	MEO-3	30 April 2012
C30	MEO-10	30 March 2018	C12	MEO-4	30 April 2012
C32	MEO-13	19 September 2018	C13	IGSO-6	30 March 2016
C33	MEO-14	19 September 2018	C14	MEO-6	19 September 2012
C34	MEO-15	15 October 2018	C16	IGSO-7	10 July 2018
C35	MEO-16	15 October 2018			
C36	MEO-17	19 November 2018			
C37	MEO-18	19 November 2018			

3. BDS/GPS Signal Characteristics

The onboard receiver has demonstrated the ability of tracking GPS and BDS signals in GEO. The flight data generated by the GNSS receiver was downloaded to the ground. In this section, we analyze the signal characteristics of BDS and GPS including observations quantity and distribution, availability, PDOP, observations accuracy.

3.1. Observations Quantity and Availability

In two days from 12:00 on 17 May to 12:00 on 19 May 2020, a total of 512,819 GPS observations and 299,523 BDS observations have been obtained at 2 s intervals. The number of GPS satellites tracked includes: 12 IIF, 11 IIR, 7 IIR-M, and 2 III satellites. The percentage of the GPS observations for IIF, IIR, IR-M, III satellites, are counted to be 27.4%, 41.4%, 27.6%, and 3.6%, respectively. The average observations of GPS III and IIF satellites are significantly less than those of the other two types of GPS satellites.

Among the 33 BDS satellites, only C01, C02 and C05 of 3 BDS GEO satellites have no observations data. The percentage of the observations from 2 BDS GEO (C03 and C04), 7 BDS IGSO, and 21 BDS MEO satellites, are counted to be 21.7%, 9.1%, 69.2%, respectively. Although the number of BDS GEO satellites tracked is only two, the observations quantity of these two satellites accounts for a large proportion.

According to results shown in Figure 3, the mean number of the GPS satellites tracked over two days is 7.4 and the mean number for the BDS satellites tracked is 4.3. Because each constellation in the receiver has only eight-channel hardware correlator, it can track up to eight satellites simultaneously. Considering the combination of GPS and BDS constellations, it remarkably increases the number of satellites tracked. The mean number for the GPS + BDS satellites tracked is 11.7. Figure 4 gives the tracking periods of the BDS satellites over two days. The BDS satellite of GEO C04 has the longest continuous tracking time, accounting for 68.9% of the two days. The continuous tracking time of the six BDS IGSO satellites is shorter than other GPS or BDS satellites.

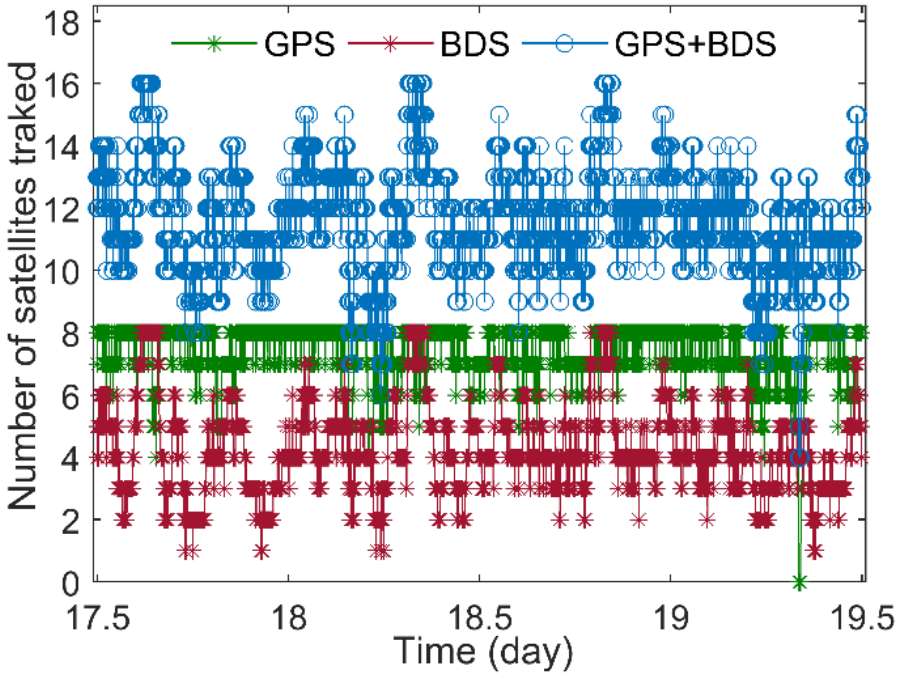

Figure 3. Number of the GPS, BDS, and GPS + BDS satellites tracked over two days.

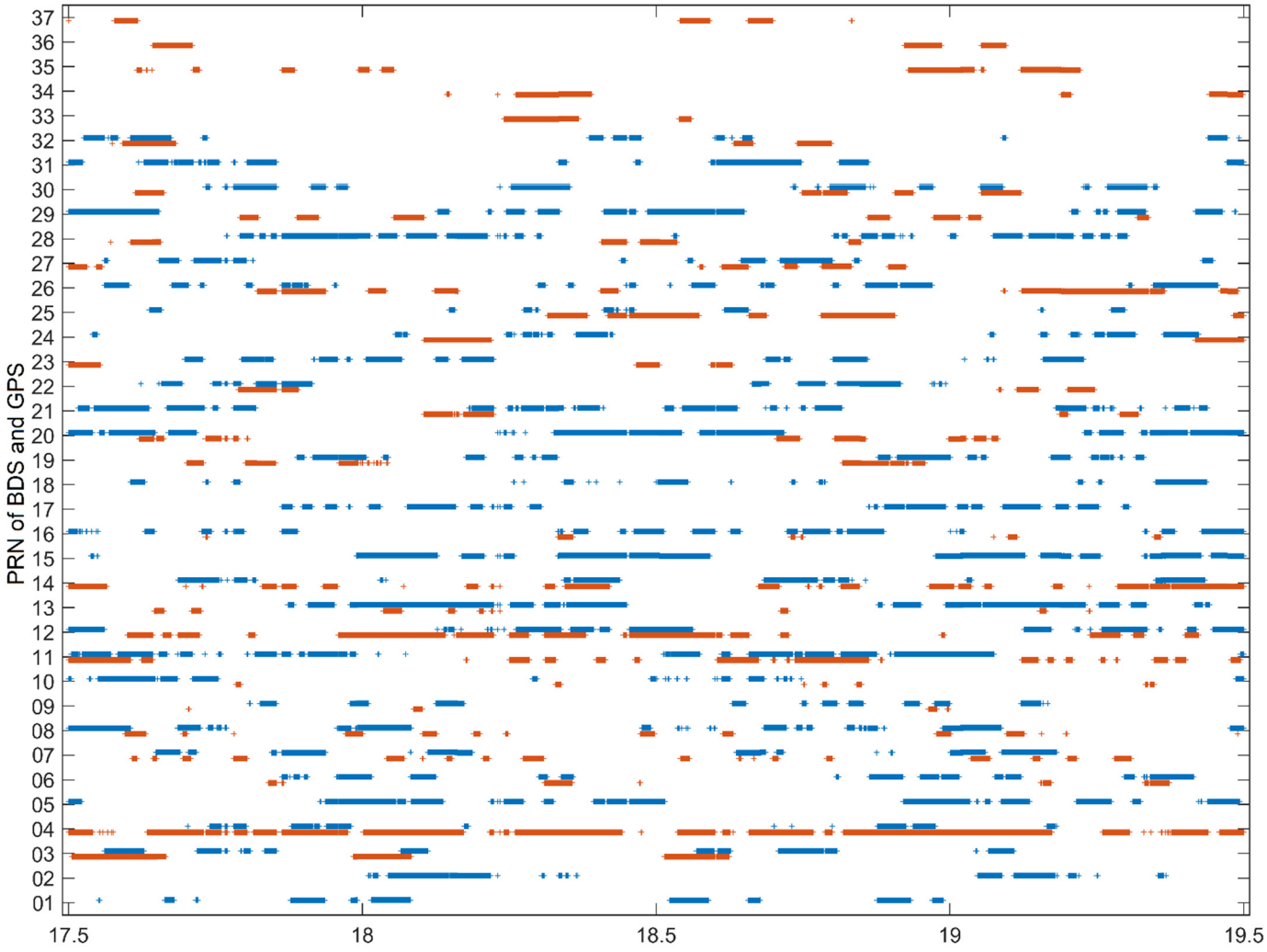

Figure 4. Availability of GPS and BDS satellites over two days (blue for GPS, brown for BDS).

3.2. PDOP

PDOP in common use is useful to characterize the accuracy of the position and velocity solutions. It can be computed based on the square root of the trace of the $\left(H^T H\right)^{-1}$ matrix. The matrix H is called as the design matrix or the Jacobian matrix and related with the least-squares solution in single point position. The matrix of H is expressed in form [27,28]

$$H = \begin{bmatrix} a_x^{i1} & a_y^{i1} & a_z^{i1} & 1 & 0 \\ a_x^{i2} & a_y^{i2} & a_z^{i2} & 1 & 0 \\ \vdots & \vdots & \vdots & \vdots & \vdots \\ a_x^{in} & a_y^{in} & a_z^{in} & 1 & 0 \\ a_x^{j1} & a_y^{j1} & a_z^{j1} & 1 & 1 \\ a_x^{j2} & a_y^{j2} & a_z^{j2} & 1 & 1 \\ \vdots & \vdots & \vdots & \vdots & \vdots \\ a_x^{jm} & a_y^{jm} & a_z^{jm} & 1 & 1 \end{bmatrix} \quad (1)$$

where n, m are the number of GPS or BDS satellites, respectively. $a_x^{in}, a_y^{in}, a_z^{in}$ denote the direction cosine vector from the receiver position of x, y, z to the nth satellite of GPS. $a_x^{jm}, a_y^{jm}, a_z^{jm}$ denote the direction cosine vector from the receiver position of x, y, z to the mth satellite of BDS. When using combination of GPS and BDS, the matrix H is a $(n + m) \times$

5, otherwise the matrix H is a $n \times 4$ and the last column in Equation (1) is ignored [27,28]. The PDOP can be obtained from

$$PDOP = \sqrt{(H^T H)^{-1}_{1,1} + (H^T H)^{-1}_{2,2} + (H^T H)^{-1}_{3,3}} \quad (2)$$

According to the Equation (1) and Equation (2), the mean value of PDOP of GPS and GPS + BDS over two days are 10.24 and 3.91, respectively. It can obviously reduce the PDOP when we use GPS + BDS constellations, as shown in Figure 5.

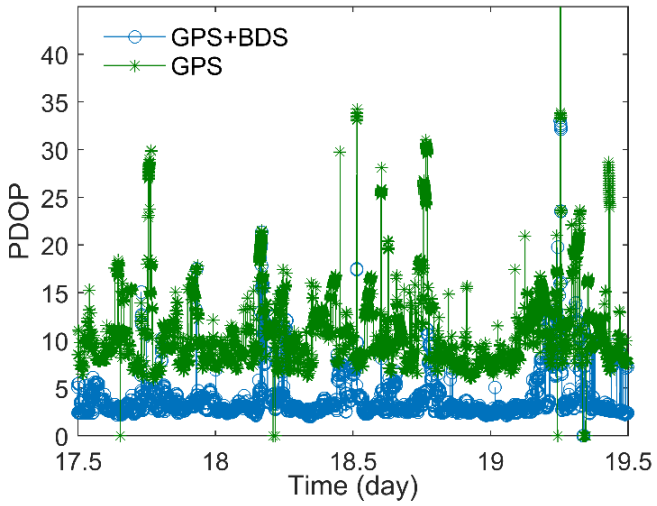

Figure 5. Values of PDOP over two days.

Sky views of the GPS and BDS satellites tracked are given in Figure 6. The nadir angles range of BDS satellites tracked is larger than that of GPS satellites tracked. Especially, the nadir angles of BDS GEO and IGSO satellites tracked are in range of 45° to 85°, which are larger than those of BDS MEO satellites tracked. This indicates that a positive contribution of BDS GEO and IGSO satellites to the improvement of PDOP is expected, although the number of these satellites tracked is not large in this mission.

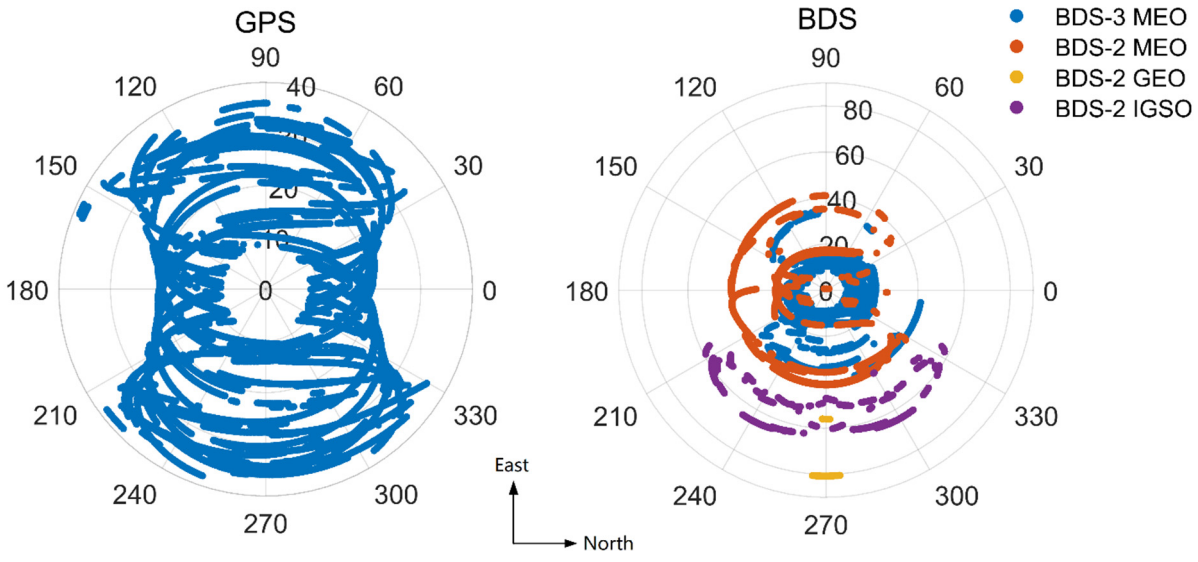

Figure 6. Sky view of GPS and BDS satellites tracked over two days with respect to azimuth and nadir angles of the receiver.

3.3. Observations Distribution and Accuracy

C/N_0 is an important indicator about the signals power, which is related to the accuracy of observations. Figure 7 gives the distribution of GPS and BDS observations with respect to C/N_0. Most of the GPS, BDS-2 IGSO, and BDS-2 MEO observations are in C/N_0 range of above 30 dB-Hz and below 35 dB-Hz. However, for BDS-3 MEO satellites, the number of observations in C/N_0 above 40 is more than that in other C/N_0 range. This indicates that most of the observations was observed from the main-lobe signals of BDS-3 MEO antenna.

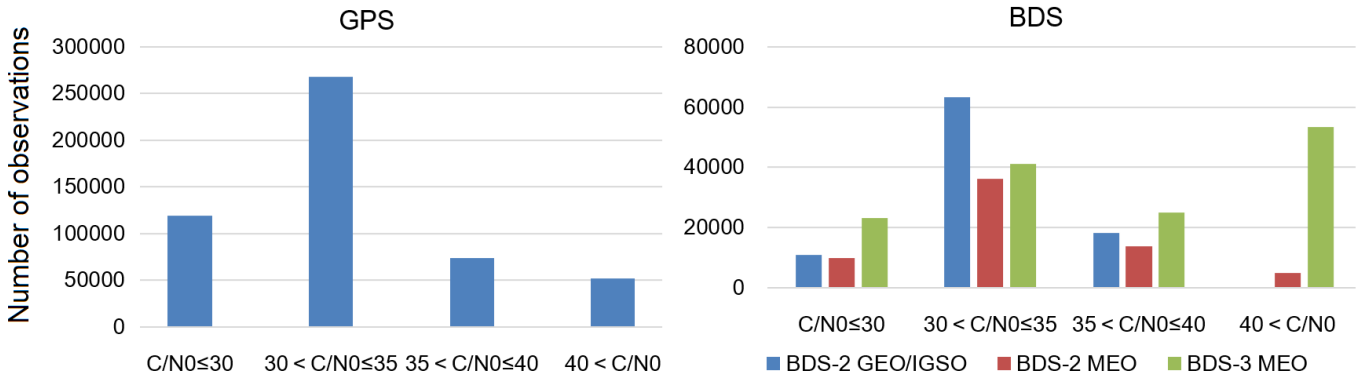

Figure 7. Distribution of observations with respect to C/N_0 over two days.

The pseudorange P_u^i and carrier phase L_u^i, respectively, are [22]

$$\begin{cases} P_u^i = \rho + c\delta t_u - c\delta t^s + \delta\rho_{trop} + \delta\rho_{iono} + \varepsilon_p^i \\ L_u^i = \rho + c\delta t_u - c\delta t^s + \delta\rho_{trop} - \delta\rho_{iono} + \lambda N_u^i + \varepsilon_L^i \end{cases} \tag{3}$$

where ρ is the geometric range between the receiver and the navigation satellite; δt^s and δt_u are navigation satellite clock offset and receiver clock offset, respectively; and c is the speed of light. $\delta\rho_{trop}$ and $\delta\rho_{iono}$ represent the troposphere and ionosphere delay errors, respectively. The parameter λN_u^i denotes the ambiguity of the carrier phase measurements. ε_p^i and ε_L^i are the measurement noises, for the pseudorange and the carrier phase, respectively. We use epoch difference arithmetics to analyze carrier phase measurement noise [22,29]. In general, only random noise remains when using triple difference, which is described as follows:

$$\begin{aligned} \Delta\varepsilon_P &= P_u^i - P_u^{i-1} - \left(P_u^{i-1} - P_u^{i-2}\right) - \left(P_u^{i-1} - P_u^{i-2} - P_u^{i-2} + P_u^{i-3}\right) \\ &= P_u^i - 3P_u^{i-1} + 3P_u^{i-2} - P_u^{i-3} \end{aligned} \tag{4}$$

$$\begin{aligned} \Delta\varepsilon_L &= L_u^i - L_u^{i-1} - \left(L_u^{i-1} - L_u^{i-2}\right) - \left(L_u^{i-1} - L_u^{i-2} - L_u^{i-2} + L_u^{i-3}\right) \\ &= L_u^i - 3L_u^{i-1} + 3L_u^{i-2} - L_u^{i-3} \end{aligned} \tag{5}$$

Therefore, we use $\Delta\varepsilon_p/\sqrt{2}$ and $\Delta\varepsilon_L/\sqrt{20}$ as the pseudorange and carrier phase noise statistics. The standard deviation of the pseudorange and carrier phase noises are shown in Figure 8. The pseudorange measurement noises are less than 4 m, and the carrier measurement noises are mostly less than 8 mm. The pseudorange and carrier phase noises of BDS measurements are lower than those of GPS measurements. Especially the pseudorange noises of BDS measurements are mostly less than 2 m in term of C/N_0 bellow 30, which are obvious lower than those of GPS measurements. According to accuracy estimation method of the code tracking errors as described in [27], the thermal noise jitter of code delay locked loop (DLL) is related to code chipping rate. Therefore, the pseudorange accuracy of BDS measurements is higher than that of GPS measurements, because the BDS B1I code chipping rate of 2046 Kbps is higher than the GPS C/A code chipping rate of 1023 Kbps.

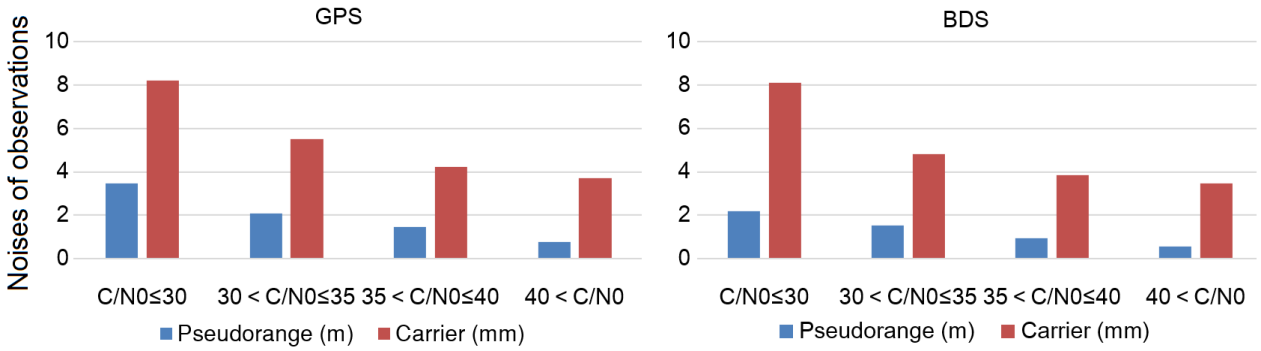

Figure 8. Standard deviation of the pseudorange noises and carrier phase noises for GPS and BDS in different C/N_0 range over two days.

4. Navigation Performance

In this section, the accuracy of single point position solutions and real-time orbit determination solutions are analyzed over two days from 9:00 on 17 May to 9:00 on 19 May 2020. No truth orbits are available as references in evaluating navigation accuracy. However, we use the precision orbit determination solutions generated on ground, which are estimated about submeter level through assessment of overlap comparisons proposed in [22].

4.1. Single-Point Position Accuracy

The single-epoch least square solutions are recalculated at 20 s intervals using flight observations and broadcast ephemerides. Comparisons between the solutions using only GPS observations and GPS + BDS observations combination at weights of 1:2, 1:1, 2:1, 4:1 and the precision orbit determination solutions are reported in Table 3. The accuracy of these solutions is related to measurement errors and the PDOP. Because the PDOP of the combined GPS+BDS satellites improves (see in Section 3.2), remarkable improvements in position and velocity accuracy are made with the combined GPS and BDS observations. When GPS observations combined with BDS observations at the weight of 1:1, the RMS of the position accuracy can improve from 32.1 m to 16.5 m and the corresponding velocity accuracy can improve from 0.238 m/s to 0.165 m/s. When BDS observations are involved, the accuracy of position and velocity in the x-axis direction is improved obviously. The x-axis direction is basically consistent with the radial direction of the orbit of the receiver, according to the location of the receiver. The position error in radial direction will be significantly higher than that in the other two directions, because there is a weak constraint in this direction [22]. According to the results in Table 3, except that the velocity differences is larger than others at weight coefficients 1:2, there is no big difference on the navigation accuracy with four different weight coefficients.

In order to evaluate the improvement obtained with BDS MEO or BDS GEO/IGSO satellites, we use GPS + BDS MEO and GPS + BDS GEO/IGSO observations combinations to calculate single-epoch least square solutions respectively. When we use GPS + BDS pseudorange combinations, one more unknown parameter (BDS clock offset) becomes available. At least two BDS satellites pseudorange combinations should be used to make sense of the BDS pseudorange contribution to the solutions. Therefore, one set of position and velocity solutions using GPS + BDS GEO/IGSO combinations are calculated when the number of BDS GEO and IGSO satellites tracked is more than or equal to two. Another set of solutions are also given using only GPS pseudorange with the same epoch as the previous set. Comparing the two sets of solutions with the reference of the precision orbit determination solutions, the position and velocity differences are reported in Table 4. In this case, using additional BDS GEO and IGSO observations reduces the position error from 28.9 m to 15.9 m and the velocity error from 0.218 m/s to 0.184 m/s.

Table 3. RMS of position and velocity differences over two days between single-epoch least square solutions with different combination weights and the reference of precision orbit determination solutions.

Items	Constellation	GPS	GPS + BDS			
	Weight	**-**	**1:2**	**1:1**	**2:1**	**4:1**
Position (m)	X	31.0	14.8	14.6	15.1	15.5
	Y	4.92	4.38	3.85	3.73	3.79
	Z	6.82	6.88	6.65	6.61	6.64
	3D	32.1	16.9	16.5	16.9	17.3
Velocity (m/s)	X	0.234	0.157	0.137	0.133	0.137
	Y	0.0339	0.0855	0.0698	0.0556	0.0656
	Z	0.0312	0.0827	0.0601	0.0450	0.0546
	3D	0.238	0.197	0.165	0.151	0.161

Table 4. RMS of position and velocity differences between single-epoch least square solutions, using only GPS observations, GPS + BDS GEO/IGSO combined, and the reference of the precision orbit determination solutions.

Results	Satellite	X	Y	Z	3D
Position (m)	GPS	28.0	4.22	6.06	28.9
	GPS + BDS GEO and IGSO	14.0	4.05	6.47	15.9
Velocity (m/s)	GPS	0.213	0.0299	0.0347	0.218
	GPS + BDS GEO and IGSO	0.106	0.0824	0.125	0.184

We use the same method to give the solutions using GPS + BDS MEO observations combinations and only GPS observations. We compare these solutions with the reference of the precision orbit determination solutions, as shown in Table 5. When using additional BDS MEO observations, the accuracy improvement in position is small and the accuracy improvement in velocity is even worse. It is further confirmed that the improvement of the position and velocity accuracy comes from combinations with BDS GEO and IGSO.

Table 5. RMS of position and velocity differences between single-epoch least square solutions, using only GPS observations, GPS + BDS MEO combined, and the reference of the precision orbit determination solutions.

Results	Satellite	X	Y	Z	3D
Position (m)	GPS	31.1	4.88	6.83	32.2
	GPS + BDS MEO	26.2	3.87	6.53	27.3
Velocity (m/s)	GPS	0.238	0.0343	0.0315	0.242
	GPS + BDS MEO	0.259	0.0570	0.0727	0.275

4.2. Real-Time Orbit Determination Accuracy

In order to improve the navigation accuracy, a real-time orbit determination filter based on an extended Kalman filter (EKF) was used with GNSS pseudorange observations and dynamic models. In the absence of observations, continuous navigation results can be calculated through orbit propagation.

4.2.1. Processing Model and Strategy

The equation of the motion of a GEO satellite can be expressed as [30]:

$$\begin{aligned} \dot{r} &= v \\ \dot{v} &= a_m(r, v, t) + w(t) \end{aligned} \tag{6}$$

where r, v, and t are the position, velocity and time of the GEO satellite in a geocentric inertial coordinate frame, respectively. a_m is the total gravity, perturbing acceleration, including the nonspherical part of the gravitational attraction of the Earth, lunisolar gravitational perturbations, solar radiation pressure, and earth tide. $w(t)$ is the empirical acceleration and can expressed in radial, along-track, and cross-track, which account for unmodeled forces. Various simplifications to the force models used in this filter are shown in Table 6, according to the reference in [31,32]. Atmospheric drag, troposphere and ionosphere delay are ignored. In this mission, we adopt the 50 × 50 order of gravity model in order to satisfy the GTO scenario of which perigee altitude is close to LEO.

Table 6. Models and parameters of onboard orbit determination used in TJS-5 mission.

Items	Description
Gravity model	EGM 2008, 50 × 50
Luni-solar gravitation	Low precision model, Moon and Sun's position are computed via analytic method
Earth tides	Low precision model, k20 solid only
Solar radiation pressure	Cannonball model, fixed effective area, C_R as estimation state
Integrator	4th-order fixed step Runge–Kutta
Integration step size	20 s
Empirical acceleration	Dynamic model compensation (DMC), τ = 60 s, σ_R:σ_A:σ_C = 200:50:50 nm/s^2
Observations	Pseudorange
Pseudorange noise	10 m
GNSS orbit and clock	Broadcast ephemeris

The state equation of EKF can be propagated by a fourth-order fixed step Runge-Kutta integrator of the adopted equation of the motion within the time update step. The filter state vector is expressed as following [30]:

$$X_{k-1} = \left[x,\ y,\ z,\ \dot{x},\ \dot{y},\ \dot{z},\ b_G,\ b_B,\ \dot{b}_u,\ C_R,\ w_R,\ w_A,\ w_C\right]^T \tag{7}$$

where $(x,\ y,\ z)$ is position vector and $(\dot{x},\ \dot{y},\ \dot{z})$ is the velocity vector, respectively. b_G is GPS clock offset, b_B is BDS clock offset, $\dot{b}_u$ is clock drift of the receiver, and C_R is the state of solar radiation pressure parameter. $(w_R,\ w_A,\ w_C)$ represents the vector of empirical accelerations in radial (R), along-track (A), and cross-track (C), respectively, which are modeled by three first-order Gauss–Markov processes to account for the unmodeled forces [33].

The observation equation of EKF can be expressed as following:

$$P_K = H_k\left(X_k - \hat{X}_k\right) + V_k \tag{8}$$

where P_K is pseudorange measurement of the ith navigation satellite. V_k is measurement noise. The measurement matrix of H_k is calculated from the linearization estimation of the pseudorange observation equation, as introduced in [34], which can be described in the following:

$$H_k = \left[\frac{\hat{x}_k - x_i^s}{\rho_i},\ \frac{\hat{y}_k - y_i^s}{\rho_i},\ \frac{\hat{z}_k - z_i^s}{\rho_i}, 0_{1\times3}, T_{1\times3}, 0, 0_{1\times3}\right] \tag{9}$$

where $(x_i^s,\ y_i^s,\ z_i^s)$ indicates the position of the ith navigation satellite, $(\hat{x}_k, \hat{y}_k, \hat{z}_k)$ is the position from predicted estimate state vector $\hat{X}_k$. $T_{1\times3}$ sets $[1,0,0]$ for GPS or $[0,1,0]$ for BDS.

4.2.2. Analysis Results

The navigation solutions are generated by a real-time orbit determination software using flight GNSS observations and broadcast ephemerides. Orbit determination filter based on EKF updates with observations at step size of 20 s. The RMS differences of position

and velocity between real-time orbit determination solutions with different pseudorange combination weights and the reference of the precision orbit determination solutions as listed in Table 7. According to the 3D results, the highest position and velocity accuracy are given at the weight of 1:1. In that case, the RMS of position differences is 5.55 m and that of position differences is 0.697 mm/s. With the increase of the weight of BDS observations, although the accuracy in x-axis direction has some improvements, the accuracy in y-axis direction and z-axis direction become worse. For instance, when GPS and BDS pseudorange combined at a weight of 1:2, the RMS of position differences in x-axis direction reduce from 7.24 m to 4.09 m. However, the corresponding differences in y-axis and z-axis direction increase by 1.06 m to 0.37 m. In detail, we give the position differences between real-time orbit determination solutions using GPS + BDS observations combinations at a weight of 1:1 and only GPS observations, and the reference of the precision orbit determination solutions, as shown in Figure 9.

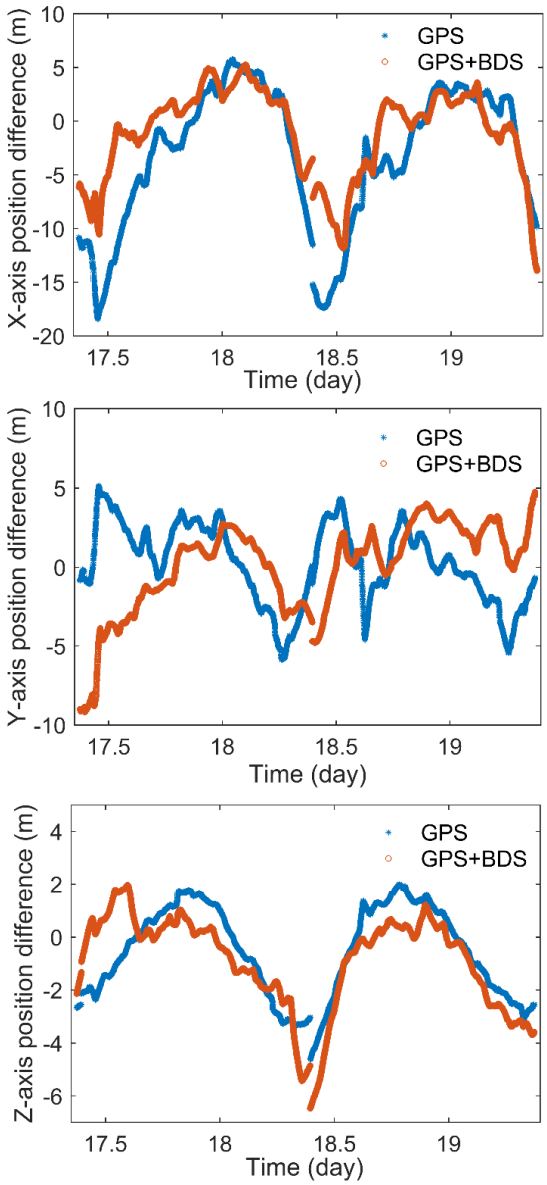

Figure 9. Position differences (x-axis, y-axis, and z-axis) over two days between real-time orbit determination solutions using GPS and GPS + BDS pseudorange with weight ratio of 1:1 and the reference of the precision orbit determination solutions.

Table 7. RMS of position and velocity differences over two days between real-time orbit determination solutions with different pseudorange combination weights and the reference of the precision orbit determination solutions.

Results		Weight (GPS + BDS)				
		GPS	**1:2**	**1:1**	**2:1**	**4:1**
Position (m)	X	7.24	4.09	4.30	5.88	6.81
	Y	2.53	3.59	2.87	1.70	1.84
	Z	1.81	2.18	2.01	1.68	1.55
	3D	7.88	5.86	5.55	6.34	7.22
Velocity (mm/s)	X	0.629	0.502	0.491	0.547	0.601
	Y	0.739	0.384	0.361	0.537	0.668
	Z	0.302	0.334	0.340	0.312	0.295
	3D	1.02	0.715	0.697	0.827	0.946

5. Conclusions

For the GEO satellite of the TJS-5 mission, we use a high sensitivity receiver with a high-gain antenna to realize real-time navigation. In this study, we analyze the inflight data generated by this sensitivity receiver, which can track weak BDS and GPS signals. We investigate the GNSS signal characteristics, including observations quantity and distribution, availability, PDOP, observations accuracy. It is found that when BDS and GPS are combined, the number of navigation satellites tracked will increase significantly and the PDOP can be reduced obviously. Although the number of BDS satellites tracked is less than that of GPS, it makes a positive contribution to the improvement of PDOP and navigation solutions. In order to analyze the observations distribution characteristics, the number of observations with respect to the C/N_0 was analyzed. Most of the GPS and BDS observations are concentrated in C/N_0 range of above 30 dB-Hz and below 35 dB-Hz, except BDS-3 MEO satellite observations. We use epoch difference arithmetics to analyze observations noises. The standard deviation of the pseudorange noises are less than 4 m, and the corresponding carrier phase noises are mostly less than 8 mm. The pseudorange and carrier phase noises of BDS measurements are lower than those of GPS measurements.

We give the navigation performance using only GPS observations and GPS + BDS observations combination at different weights. As for the single-epoch least square solutions, remarkable improvements in position and velocity accuracy are made with the combined GPS and BDS observations. Through comparisons with the precision reference orbits, when combining GPS observations with BDS observations at the weight of 1:1, the RMS of these position solutions accuracy can improve from 32.1 m to 16.5 m and the corresponding velocity accuracy can improve from 0.238 m/s to 0.165 m/s. Especially in x-axis direction, the position accuracy can improve from 31.0 m to14.6 m. We discuss the accuracy influence when BDS GEO/IGSO and MEO combined with GPS respectively. In this case, when BDS IGSO and GEO observations involved, there is an obvious improvement in position and velocity. As for the real-time orbit determination solutions, the RMS of position accuracy is 5.55 m and that of velocity accuracy is 0.697 mm/s when GPS and BDS pseudorange combined at a weight of 1:1. When we increase the weight of BDS observations, although the accuracy in x-axis direction has some improvements, the accuracy in y-axis direction and z-axis direction become worse.

We need to do further research into some aspects to improve the accuracy in future high-earth-orbit missions. A comprehensive utilization of GPS, GLONASS, BDS and GALILEO system should be taken into account to improve orbit determination accuracy by increasing the number of available satellites and reducing PDOP. In addition, carrier observations should be considered to increase navigation accuracy, because the accuracy of carrier observations is higher than that of pseudorange observations. For the high-orbit satellites with orbit maneuver, the research on how to use IMU to realize integrated navigation is necessary.

Author Contributions: Conceptualization, M.W.; methodology, M.W. and T.S.; software, M.W. and W.Z.; validation, M.W. and T.S.; formal analysis, M.W. and H.H.; investigation, M.W. and W.Z.; resources, M.W.; data curation, M.W.; writing—original draft preparation, M.W. and T.S.; writing—review and editing, M.W.; visualization, M.W.; supervision, H.H.; project administration, H.H.; funding acquisition, W.Z. All authors have read and agreed to the published version of the manuscript.

Funding: This work was supported by the National Natural Science Foundation of China (NSFC) under Grant Nos. 62073044.

Data Availability Statement: The data that support the findings of this study are available from the corresponding author upon reasonable request.

Acknowledgments: The authors would like to acknowledge the IGS for providing the broadcast ephemeris and GNSS Research Center of Wuhan University providing precision orbit determination solutions.

Conflicts of Interest: The authors declare no conflict of interest.

References

1. Jorgensen, P. Autonomous navigation of geosynchronous satellites using the NAVSTAR global positioning system. In Proceedings of the National Telesystems Conference, Galveston, TX, USA, 1–7 December 1982.
2. Bauer, F.H.; Moreau, M.C.; Dahle-Melsaether, M.E.; Petrofski, W.P.; Stanton, B.J.; Thomason, S.; Harris, G.A.; Sena, R.P.; Parker, L. The GPS space service volume. In Proceedings of the 19th International Technical Meeting of the Satellite Division of The Institute of Navigation (ION GNSS 2006), Fort Worth, TX, USA, 26–29 September 2006.
3. Bauer, F.H.; Parker, J.J.K.; Welch, B.; Enderle, W. Developing a robust, interoperable GNSS space service volume (SSV) for the global space user community. In Proceedings of the ION ITM 2017, Monterey, CA, USA, 30 January–2 February 2017; pp. 132–149.
4. Parker, J.J.K.; Bauer, F.H.; Ashman, B.W.; Miller, J.J.; Enderle, W.; Blonski, D. Development of an Interoperable GNSS Space Service Volume. In Proceedings of the 31st International Technical Meeting of the Satellite Division of the Institute of Navigation (ION GNSS+ 2018), Miami, FL, USA, 24–28 September 2018; pp. 1246–1256. [CrossRef]
5. Lin, K.; Zhan, X.Q.; Yang, R.; Shao, F.W.; Huang, J.H. BDS Space Service Volume characterizations considering side-lobe signals and 3D antenna pattern. *Aerosp. Sci. Technol.* **2020**, *106*, 106071. [CrossRef]
6. Shuai, J.; Zhan, X.Q.; Lu, J.; Feng, S.J.; Ochieng, W.Y. Characterisation of GNSS Space Service Volume. *J. Navig.* **2015**, *68*, 107–125.
7. Ruiz, J.L.; Frey, C.H. Geosynchronous Satellite Use of GPS. In Proceedings of the 18th International Technical Meeting of The Satellite Division of the Institute of Navigation (ION GNSS 2005), Long Beach, CA, USA, 13–16 September 2005; pp. 1227–1232.
8. Force, D.A.; Miller, J.J. Combined Global Navigation Satellite Systems in the Space Service Volume. In Proceedings of the International Technical Meeting 2013, San Diego, CA, USA, 27–29 January 2013.
9. Rathinam, A.; Dempster, A.G. Effective utilization of space service volume through combined GNSS. In Proceedings of the 29th International Technical Meeting of the Satellite Division of the Institute of Navigation (ION GNSS+ 2016), Portland, OR, USA, 12–16 September 2016.
10. Parker, J.; Valdez, J.; Bauer, F.; Moreau, M. Use and protection of GPS side lobe signals for enhanced navigation performance in high Earth orbit. In Proceedings of the 39th Annual American-Astronautical-Society Rocky Mountain Section Guidance, Navigation and Control Conference, Breckenridge, CO, USA, 5–10 February 2016; pp. 329–341.
11. King, M. Extending the use of GPS to geostationary altitudes. In Proceedings of the AIAA SPACE 2011 Conference & Exposition, Long Beach, CA, USA, 27–29 September 2011; pp. 1–9. [CrossRef]
12. Czopek, F.M. Description and Performance of the GPS Block I and II L-Band Antenna and Link Budget. In Proceedings of the 6th International Technical Meeting of the Satellite Division of The Institute of Navigation (ION GPS 1993), Salt Lake City, UT, USA, 22–24 September 1993; pp. 37–43.
13. Lorga, J.M.; Silva, P.F.; Cintio, D.A.; Dovis, F.; Kowaltschek, S.; Jimenez, D.; Jansson, R. GNSS sensor for autonomous orbit determination. In Proceedings of the 23rd International Technical Meeting of the Satellite Division of the Institute of Navigation, Portland, OR, USA, 21–24 September 2010; pp. 2717–2731.
14. Mikhaylov, N.V.; Koshaev, D.A. Navigation solution for a geostationary satellite based on its dynamic equations and occasional gnss measurements. *Gyroscopy Navig.* **2015**, *6*, 87–100. [CrossRef]
15. Marmet, F.X.; Maureau, J.; Calaprice, M. GPS/Galileo navigation in GTO/GEO orbit. *Acta Astronaut.* **2015**, *117*, 263–276. [CrossRef]
16. Capuano, V.; Shehaj, E.; Blunt, P.; Botteron, C.; Farine, P.A. High accuracy GNSS based navigation in GEO. *Acta Astronaut.* **2017**, *136*, 332–341. [CrossRef]
17. Ebinuma, T.; Unwin, M. GPS receiver demonstration on a Galileo test bed satellite. *Navigation* **2007**, *60*, 349–362. [CrossRef]
18. Unwin, M.; Steenwijk, R.D.V.V.; Blunt, P.; Hashida, Y.; Kowaltschek, S.; Price, S.R. Navigating Above the GPS Constellation-Preliminary Results from the SGR-GEO on GIOVE-A. In Proceedings of the 26th International Technical Meeting of The Satellite Division of the Institute of Navigation (ION GNSS+ 2013), Nashville, TN, USA, 16–20 September 2013; pp. 3305–3315.

19. Chapel, J.; Stancliffe, D.; Bevacqua, T.; Winkler, S.; Clapp, B.; Rood, T. Guidance, navigation, and control performance for the goes-r spacecraft. *Ceas Space J.* **2015**, *7*, 87–104. [CrossRef]
20. Winkler, S.; Ramsey, G.; Frey, C.; Chapel, J.; Chu, D.; Freesland, D.; Krimchansky, A.; Concha, M. GPS receiver on-orbit performance for the GOES-R spacecraft. In Proceedings of the 10th International ESA Conference on GNC Systems, Salzburg, Austria, 29 May–2 June 2017.
21. Neumann, N.; Dd Bruijn, F.; Lübke-ossenbeck, B.; Marx, M.; Gottzein, E.; Dauphin, H.; Chamarro, M.S. In-flight results from the GPS receiver on Small GEO. In Proceedings of the 68th International Astronautical Congress, Adelaide, Australia, 25–29 September 2017.
22. Jiang, K.; Li, M.; Wang, M.; Zhao, Q.; Li, W. TJS-2 geostationary satellite orbit determination using onboard GPS measurements. *GPS Solut.* **2018**, *22*, 87. [CrossRef]
23. Capuano, V.; Blunt, P.; Botteron, C.; Tian, J.; Leclère, J.; Wang, Y.G.; Basile, F.; Farine, P. Standalone GPS L1 C/A receiver for lunar missions. *Sensors* **2016**, *16*, 347. [CrossRef]
24. Manzano-Jurado, M.; Alegre-Rubio, J.; Pellacani, A.; Seco-Granados, G.; López-Salcedo, J.A.; Guerrero, E.; García-Rodríguez, A. Use of weak GNSS signals in a mission to the moon. In Proceedings of the 7th ESA Workshop on Satellite Navigation Technologies and European Workshop on GNSS Signals and Signal Processing (NAVITEC), Noordwijk, The Netherlands, 3–5 December 2014; pp. 1–8. [CrossRef]
25. Li, M.; Yuan, Y. Estimation and Analysis of BDS2 and BDS3 Differential Code Biases and Global Ionospheric Maps Using BDS Observations. *Remote Sens.* **2021**, *13*, 370. [CrossRef]
26. Hein, G.W. Status, perspectives and trends of satellite navigation. *Sat. Navig.* **2020**, *1*, 22. [CrossRef]
27. Kaplan, E.D.; Hegarty, C.J. *Understanding GPS: Principles and Applications*, 2nd ed.; Artech House Inc.: Boston, MA, USA, 2005.
28. Teng, Y.; Wang, J.; Qi, H. Minimum of Geometric Dilution of Precision (GDOP) for five satellites with dual-GNSS constellations. *Adv. Space Res.* **2015**, *56*, 229–236. [CrossRef]
29. Kirkko-Jaakkola, M.; Traugott, J.; Odijk, D.; Collin, J.; Sachs, G.; Holzapfel, F. A RAIM approach to GNSS outlier and cycle slip detection using L1 carrier phase time-differences. In Proceedings of the IEEE Workshop on Signal Processing Systems, SiPS 2009, Tampere, Finland, 7–9 October 2009; pp. 273–278. [CrossRef]
30. Wang, F.; Gong, X.; Sang, J.; Zhang, X. A Novel Method for Precise Onboard Real-Time Orbit Determination with a Standalone GPS Receiver. *Sensors* **2015**, *15*, 30403–30418. [CrossRef]
31. Montenbruck, O.; Gill, E. *Satellite Orbits: Models, Methods and Application*; Springer: Berlin, Germany, 2000.
32. Gong, X.; Sang, J.; Wang, F.; Li, X. LEO onboard real-time orbit determination using GPS/BDS data with an optimal stochastic model. *Remote Sens.* **2020**, *12*, 3458. [CrossRef]
33. Goldstein, D.B. Real-time, Autonomous Precise Satellite Orbit Determination Using the Global Positioning System. Ph.D. Thesis, University of Colorado, Boulder, CO, USA, 2000.
34. Tapley, B.D.; Schutz, B.E.; Born, G. *Statistical Orbit Determination*; Elsevier: Amsterdam, The Netherlands, 2004.